ACS APPLIED MATERIALS & INTERFACES

Research Article

www.acsami.org

Controlling Dielectric and Relaxor-Ferroelectric Properties for Energy Storage by Tuning $Pb_{0.92}La_{0.08}Zr_{0.52}Ti_{0.48}O_3$ Film Thickness

Emery Brown,[†] Chunrui Ma,[‡] Jagaran Acharya,[‡] Beihai Ma,[§] Judy Wu,*[,‡] and Jun Li*[,†]

[†]Department of Chemistry, Kansas State University, 213 CBC Building, Manhattan, Kansas 66506, United States

[‡]Department of Physics and Astronomy, University of Kansas, 1082 Malott, 1251 Wescoe Hall Drive, Lawrence, Kansas 66045, United States

[§]Energy Systems Division, Argonne National Laboratory, 9700 S. Cass Avenue, Argonne, Illinois 60439, United States

Supporting Information

ABSTRACT: The energy storage properties of $Pb_{0.92}La_{0.08}Zr_{0.52}Ti_{0.48}O_3$ (PLZT) films grown via pulsed laser deposition were evaluated at variable film thickness of 125, 250, 500, and 1000 nm. These films show high dielectric permittivity up to ~1200. Cyclic $I-V$ measurements were used to evaluate the dielectric properties of these thin films, which not only provide the total electric displacement, but also separate contributions from each of the relevant components including electric conductivity ($D1$), dielectric capacitance ($D2$), and relaxor-ferroelectric domain switching polarization (P). The results show that, as the film thickness increases, the material transits from a linear dielectric to nonlinear relaxor-ferroelectric. While the energy storage per volume increases with the film thickness, the energy storage efficiency drops from ~80% to ~30%. The PLZT films can be optimized for different energy storage applications by tuning the film thickness to optimize between the linear and nonlinear dielectric properties and energy storage efficiency.

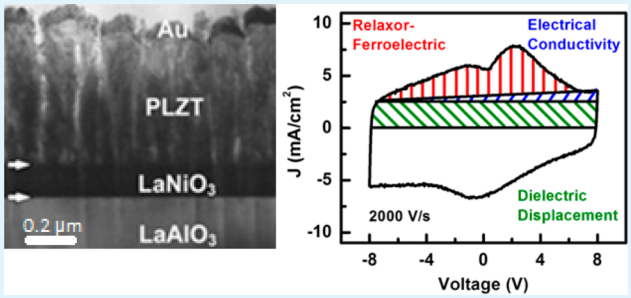

KEYWORDS: *solid-state dielectric capacitors, relaxor ferroelectrics, energy storage, PLZT film*

INTRODUCTION

Electrical energy storage (EES) devices are critical for powering portable electronics and supporting renewable energy technologies. Current commercial EES devices include batteries, dielectric capacitors, and electrochemical capacitors (or supercapacitors). Among them, solid-state dielectric capacitors have distinctly high power densities, very large operation voltages, and a long cycle life. The simple structure, small footprint, low package volume, and ease in fabrication make them particularly suitable for integration into microelectronics which requires fast charge−discharge (in milliseconds or smaller time scale) for short-term power regulation. Conventional dielectric capacitors are based on linear properties, i.e., the stored charge Q is proportional to the product of the capacitance C and the applied voltage V by $Q = CV$ with C being a constant over the applied voltage range. However, the energy density of such linear dielectric capacitors is low (~10^{-2} to 10^{-1} W h/kg) compared with other EES technologies.[1] One solution to this problem is employing materials with higher dielectric constant ε_r to achieve higher areal specific capacitance C_0 as defined by $C_0 = \varepsilon_0\varepsilon_r/d$ with ε_0 being the vacuum permittivity and d the dielectric film thickness. Among possible candidates, ferroelectric materials have attracted extensive attention due to the orders-of-magnitude higher dielectric constant ε_r than that of conventional dielectric materials.[1−3] Interestingly, they present distinctive nonlinear dielectric properties with ε_r (and C_0) significantly dropping at high voltage bias V (or the electric field E). Consequently, the energy storage mechanism in ferroelectric capacitors is quite different from conventional dielectric capacitors.[1,3]

Common ferroelectric films used for capacitors include polymers such as poly(vinylidene fluoride) (PVDF)[1,4−6] and ceramics,[1−3,7,8] whose internal polarization states associated with the orientation of dipole moment of individual domains can be reversed under an external electric field. The domain switching is represented by the characteristic hysteresis loop in the polarization-electric field ($P-E$) curve where the polarization P is the total charge involved in the process. The term P is simplified as Q in earlier discussion on linear dielectric capacitors. Ceramic films are particularly attractive due to their higher ε_r value than polymers (~1000 vs ~100 or less), superior mechanical and thermal properties, larger temperature range for operation, and high breakdown field E_b. However, for energy storage, the hysteresis $P-E$ loop needs to be suppressed in order to reduce the energy loss and therefore enhance the overall efficiency. The need for increased efficiency has

Received: September 19, 2014
Accepted: November 18, 2014
Published: November 18, 2014

motivated efforts of exploring relaxor-ferroelectric materials, a subclass of ferroelectrics.[9] Like normal ferroelectrics, relaxor-ferroelectric materials present a permanent dipole moment in individual domains.[7,9,10] However, their domain sizes are on the order of nanometers instead of micrometers like those of typical ferroelectric materials. Thus, it takes much less energy to align the dipole moment with the external electric field, leading to smaller coercive field E_c and lower remnant polarization P_r in the typical $P-E$ loop.[1,3,10]

One type of particularly interesting ceramic relaxor-ferroelectric material is lanthanum-doped lead zirconium titanate (PLZT),[11,12] an A-site substituted form of lead zirconate titanate (PZT). It is a well-known member of the perovskite family and shows great potential in applications such as nonvolatile random access memories, microwave devices, and electromechanical or photomechanical transducers.[13−15] In particular, research has been focused on its energy storage ability owing to its high permittivity and low remnant polarization.[3,12,16] Hao et al. reported an energy density up to 28.7 J/cc and with an areal capacitance density of 925 nF/cm^2 for 1 μm thick $Pb_{0.91}La_{0.09}(Ti_{0.65}Zr_{0.35})O_3$ (PLZT 9/65/35) films on platinum-buffered silicon substrates.[12] Tong et al. obtained comparable results with a maximum energy density of 22 J/cc with an electrical energy storage efficiency of 77% for a 3 μm $Pb_{0.92}La_{0.08}(Zr_{0.52}Ti_{0.48})O_3$ (PLZT 8/52/48) film deposited on a lanthanum nickel oxide buffer layer covered nickel substrate (LNO/Ni).[3] These results show very high energy storage capabilities approaching that of electrochemical capacitors. However, the PLZT films in both studies were produced via sol−gel methods which often introduce defects during the fabrication process, such as residual fine pores, hydroxyls, and cracking during the drying stage. Moreover, many sol−gel methods require long fabrication time, large amount of precursors, and high cost for materials which may make them inadequate for large scale production.

Here we report the study of energy storage properties of high-quality epitaxial PLZT (8/52/48) thin films (from ∼100 to 1000 nm) grown by pulsed laser deposition (PLD), a potentially scalable technique. These PLZT films contain substatially fewer crystallographic defects, especially a reduction in the number of large-angle grain boundaries.[17−19] However, since the thickness is near the scale of grain boundaries, the current passing through these PLZT films contains significant leakage current due to the finite electric conductivity[8,20,21] and capacitive charge−discharge current due to the linear dielectric permittivity,[22,23] which are superimposed with the conventional polarization measurement due to relaxor-ferroelectric domain switching as observed in thicker films. The relative contributions from each component should depend on the film thickness. The leakage current and linear dielectric charge−discharge current should decrease when the film thickness is increased, and the complicated nonlinear ferroelectric current should begin to dominate. It is difficult, perhaps even impossible, to separate the three components of leakage, charge−discharge, and nonlinear ferroelectric current using conventional $P-E$ measurements. Therefore, we adapt a method based on cyclic current−voltage ($I-V$) measurements by applying triangular voltage waveforms using simple potentiostats. The contributions of three components are extracted on the basis of their characteristic $I-V$ features as described by Yan et al.[22] Our results reveal that, for PLZT thickness increasing from 125 to 250, 500, and 1000 nm, PLZT transits from an approximately linear dielectric to a largely nonlinear relaxor-ferroelectric behavior. Accordingly, the energy storage density and efficiency are significantly altered. This result is important toward understanding the energy storage properties of the PLZT thin films and to the best of our knowledge, this is the first work to use the cyclic $I-V$ method to investigate the energy storage capability of a relaxor-ferroelectric thin film.

EXPERIMENTAL SECTION

PLZT films were grown at 650 °C under 225 mTorr oxygen partial pressure on (001) Nb doped STO (Nb:STO) or (100) $LaNiO_3$ (LNO), which also serves as the bottom electrode, on $LaAlO_3$ substrate using a pulsed laser deposition (PLD) system with KrF excimer laser (wavelength of 248 nm and pulse width of 25 ns) as described before.[19] The average laser pulse energy density was 2 J/cm^2 with laser repetition rate of 10 Hz. After deposition, the films were *in situ* annealed at 600 Torr oxygen and 650 °C for half an hour to reduce oxygen vacancies before cooling down to room temperature. Top electrodes were formed using 10 nm Pt followed by 80 nm Au deposited by electron-beam evaporation through a shadow mask to define 400-μm-diameter circular electrode area. X-ray diffraction (XRD) profiles were taken using a Bruker AXS D8 diffraction system. The topography of the PLZT film was measured with an atomic force microscope in tapping mode (WiTec Alpha300, Germany).

For validation of the ferroelectric properties, the PLZT films were first measured using the conventional method with a Radiant Premier II tester (Albuquerque, NM) at 100 Hz with an applied electric field of −160 to 160 kV/cm. The data are presented in the form of a typical $P-E$ hysteresis loop in Figure S1a of Supporting Information. Permittivity and dielectric loss, as shown in Supporting Information Figure S1b, were measured at 10 kHz with an Agilent E4980A Precision LCR Meter.

Cyclic $I-V$ measurements of 125 and 250 nm PLZT films were conducted using a 760E Bipotentiostat (CH Instruments Inc., Austin, TX) and those for the thicker PLZT films (500 nm and 1 um) using a PARSTAT 2273 Analyzer (Princeton Applied Research Corporation, Oakridge, TN). The voltage range for each instrument above is about ±6 V and ±10 V, respectively. All measurements were conducted in a two-electrode setup with the bottom electrode connected through a copper plate underneath the sample. A tungsten microprobe was brought into contact with the top electrode using a XYZ Micromanipulator (Quarter Research, Bend, OR). The voltage ramping rate υ of the triangular waveform was fixed at a value between 100 and 2000 V/s. The electric displacement D was calculated by dividing the integrated area under the $I-V$ curve with υ and present in $D-E$ loops.

RESULTS AND DISCUSSION

X-ray diffraction confirmed the PLZT films are (001)-oriented epitaxial with the in-plane (100) and (010) axes aligned with that of Nb:STO or LNO electrode layers, as shown in Figure 1a. The XRD $\theta-2\theta$ profile was measured with a tilt angle at 45° with respect to the normal of the film. The average surface roughness of PLZT film is around 10 nm over an area of 10 × 10 μm^2 from atomic force microscopy measurement as shown in Figure 1b. A TEM image of the lateral view of a representative 500 nm PLZT film sample in Figure 1c shows the exact thickness and columnar structure.

Figure 2a shows a typical $P-E$ loop for the 500 nm PLZT film measured with the conventional Radiant Premier II tester at 100 Hz between an applied field of −160 to 160 kV/cm (i.e., E_{max} = 160 kV/cm). The shape of the hysteresis loop validates that the PLD grown PLZT film behaves as a relaxor-ferroelectric material under such unsaturated polarization conditions, as described within previous publications.[3,10] The values of the coercive field E_c and remnant polarization P_r are 24 kV/cm and 3.6 μC/cm^2, respectively, which are slightly

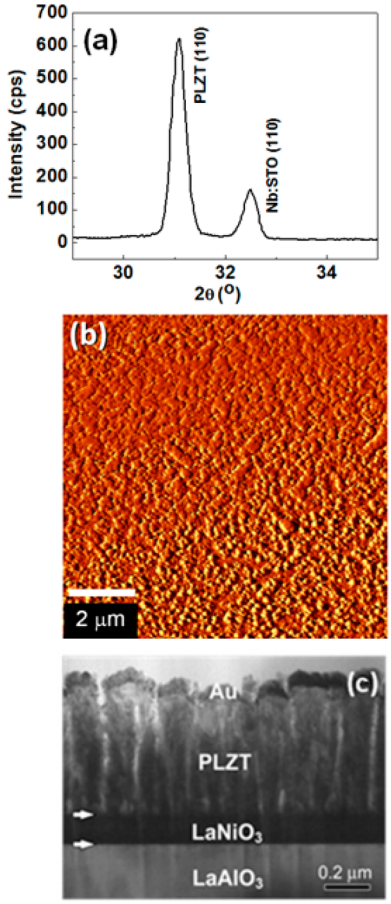

Figure 1. (a) X-ray diffraction pattern of PLZT deposited by pulsed laser deposition on Nb:STO substrate measured with a 45° tilt angle. (b) Topographic image by atomic force microscope of the PLZT film. (c) A transmission electron microscopy image of the cross-sectional view of the PLZT film.

smaller than those reported values of 1-μm-thick PLZT film by a sol–gel process under the similar E_{max}.[12] The observed higher nonlinearity is attributed to the high domain mobility in epitaxial PLZT thin films.[19]

The energy storage properties of the thin-film PLZT are schematically illustrated in Figure 2b with quadrant I of the P–E loops for the 500 nm (1) and 125 nm (2) PLZT films. The shaded region between the discharge loop and the line at max polarization P_{max} represents the recoverable electrical energy density U_{reco} in units of J/cc, which can be calculated by integrating the area between P_r and P_{max} by[1,3,10,11]

$$U_{reco} = \int_{P_{max}}^{P_r} E \, dP \tag{1}$$

The total energy stored U_{store} can be determined in a similar way by integrating the area between the charging polarization curve and the P_{max} line, which consists of the shaded region plus the area inside the loop. The electrical energy storage efficiency η is thus determined by

$$\eta = \frac{U_{reco}}{U_{store}} \times 100\% \tag{2}$$

Since the permittivity is defined by the general relationship $\varepsilon_0\varepsilon_r = dP/dE$, the recoverable electrical energy density can be defined as

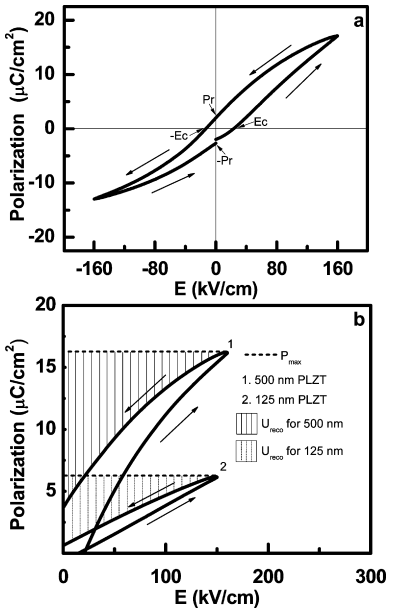

Figure 2. (a) P–E hysteresis loop of the 500 nm PLZT film measured using the conventional method and a Radiant Premier II tester shows the representative relaxor-ferroelectric behavior with characteristic coercive field (E_c and $-E_c$) and remnant polarization (P_r and $-P_r$). (b) Schematic illustration of the energy storage characteristics obtained using the P–E hysteresis loops of a 500 nm PLZT film (curve 1) in comparison with a 125 nm PLZT film (curve 2).

$$U_{reco} = \int_{E_{max}}^{0} \varepsilon_0\varepsilon_r E \, dE \tag{3}$$

For a relaxor-ferroelectric material, ε_r is a function of E. As shown in Supporting Information Figure S1b, the 500 nm PLZT film presents a very high ε_r (~1300) that peaked at the electric field around E_c and quickly drops to ~650 at E = 100 kV/cm. The permittivity curves shift in opposite direction in correlation with the P–E loop in Figure 2a and Supporting Information Figure S1a. In contrast, in a linear dielectric capacitor, the P–E loop diminishes, and thus the stored energy can be completely recovered. In addition, the polarization curve superimposes onto a straight line with $P = C_0V = C_0Ed = \varepsilon_0\varepsilon_r E$, where $C_0 = (\varepsilon_0\varepsilon_r)/d$ is the area-specific capacitance. Incorporating this result within eq 3 gives the simple and commonly known formula for volume-specific energy density of linear dielectric capacitors:

$$U = \left(\frac{1}{2}C_0V^2\right)/d = \left(\frac{1}{2}C_0E^2\right) \times d \tag{4}$$

Unfortunately, the linear dielectric capacitor is limited in energy storage, which is typically several orders of magnitude smaller than for some materials, due to the much lower ε_r. It is of interest to investigate how the dielectric properties of the PLZT films can be tailored by tuning the film thickness so that optimum energy storage properties can be achieved within the material system as it transits form a linear dielectric to relaxor ferroelectric.

It should be noted that the polarization P in the P–E curves shown in Figure 2 and Supporting Information Figure S1a should be more precisely referred to as electric displacement D, which consists of three contributions: electric conductivity $D1$, dielectric capacitance $D2$, and domain switching ferroelectric polarization P.[22] In conventional thick ferroelectric films, $D1$

and *D2* are negligible, and thus, only *P* is presented. For thin relaxor-ferroelectric films with the thickness less than 1000 nm, the leakage current (*D1*)[8,20,21] and dielectric capacitive current (*D2*)[22,23] become significant since both are inversely proportional to the film thickness. For relaxor-ferroelectric thin films, the nanoscale grain structure and defects make them highly susceptive to leakage current, and high ε_r values make the dielectric capacitance significant (with $C_0 = (\varepsilon_0\varepsilon_r)/d$). However, conventional *P*–*E* measurements only record the total *D* and are inadequate for providing insights into the individual factors.

This issue can be resolved using cyclic *I*–*V* measurements using a triangular voltage waveform, as described by Yan et al.[22] The contributions of all three components can be separated by their characteristic *I*–*V* features illustrated in Figure 3. Figure 3a,b shows the *I*–*V* curves at scan rate υ of 500, 1000, and 2000 V/s from two representative PLZT films with 125 and 500 nm thickness, respectively. *I*–*V* characteristics for all four film thickness (125, 250, 500, and 1000 nm) are shown in Supporting Information Figure S2 for direct comparison. The measurements were conducted at about ±2 V and ±8 V, respectively, to maintain the same maximum electric field E_{max} at ±160 kV/cm (below the breakdown field E_b as shown in Supporting Information Figure S3). Clearly, the *I*–*V* curve from a completed cycle of the 125 nm PLZT film presents a shape close to a rectangular box, which is characteristic of simple linear dielectric capacitors. In contrast, the *I*–*V* curve of the 500 nm PLZT film is dominated by a pair of broad waves that peaked at ~2.0 V in the forward scan and at ~0.5 V in the reverse scan. The electric displacement *D* can be calculated by integrating the area under the *I*–*V* curve and then dividing by the scan rate υ. For clear view, the contributions of *D1*, *D2*, and *P* are marked by different shaded areas under the forward scan curve at 2000 V/s for both samples.

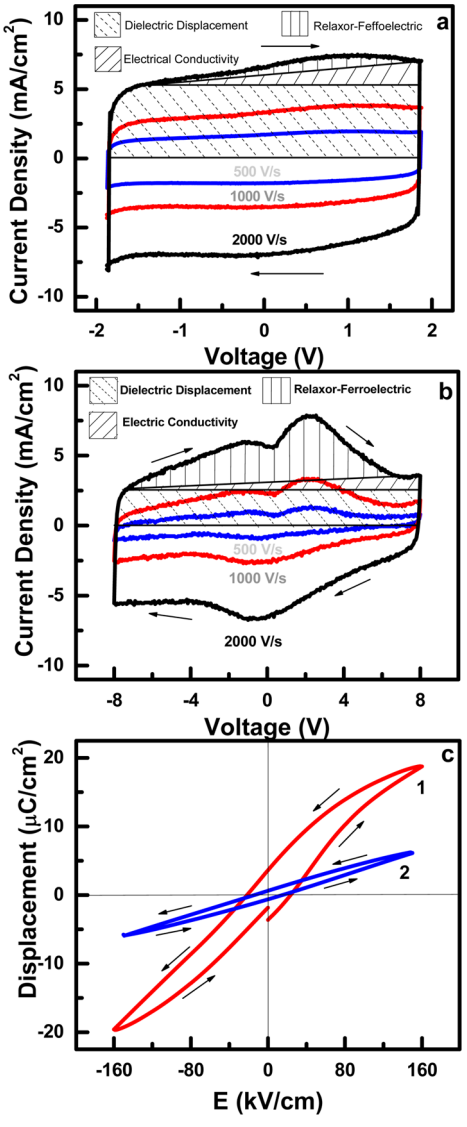

Figure 3. Cyclic *I*–*V* curves for the 125 nm (a) and 500 nm (b) PLZT films, depicting the contributions to the total dielectric displacement by electric conductivity *D1*, linear dielectric capacitance *D2*, and relaxor-ferroelectric domain switching polarization *P*. The measurements were performed by applying triangular waveforms at a constant cycling rate of 500, 1000, and 2000 V/s, respectively. (c) The electric displacement to electric field (*D*–*E*) loops for the 500 nm (curve 1) and 125 nm (curve 2) PLZT films derived by integrating the charges under the *I*–*V* curves.

The *I*–*V* curve of an ideal linear dielectric capacitor should be a rectangular box except for small rounding at the two voltage limits due to the RC delay when the polarity is reversed. The magnitude of the current density is a constant during the scan and is proportional to the scan rate (i.e., $i_0 = C_0 \times \upsilon$). Indeed, the baseline current density in both parts a and b of Figure 3 linearly increases with the scan rate. The *D2* contribution is much larger in 125 nm PLZT film than that in the 500 nm one. For both PLZT samples, the baseline has a slope. The slope of the line can be extrapolated from the two ends of the *I*–*V* curve to add a triangular area attributed to *D1* on top of the dielectric boxes. The straight line is simply the Ohmic effect due to the electric conductivity of the PLZT film. From the slope of the baseline, the resistivity ρ of the PLZT film can be calculated to be 1.6×10^8 and 2.9×10^8 Ω cm for 125 and 500 nm, respectively. These values are smaller than ~8.3×10^{10} Ω cm resistivity of the sol–gel deposited 1-μm PLZT film derived from the stable leakage current in a previous study.[12] It is worth noting that the dynamic current at high scan rate (2000 V/s) is expected to be nearly 10 times higher.[12] The high crystallinity of the PLZT film by PLD may also give higher conductivity.[19]

The remaining area under the *I*–*V* curve is from the wave feature attributed to domain switching polarization *P*. This area is rather small in the 125 nm PLZT film but becomes prominent in the 500 nm PLZT film. The shape and peak voltage of the *I*–*V* waves in the 500 nm sample is sensitive to the history and the voltage bias conditions V_{max}, but its peak area remains about the same and proportionately increases with the scan rate υ. The domain switching peaks in the charging and discharging cycles, however, are not symmetric to zero voltage with values of ~2.0 and −0.5 V, respectively, indicating an asymmetrical pull of domain switching between the charging and discharging cycles. This is likely due to voltage and charge offsets by effects of strain gradient as a result of epitaxial stresses when sandwiched between two different substrates or electrode materials.[24,25] The asymmetrical *I*–*V* feature is even more prominent with the 1000 nm PLZT film showing peaks at ~7.0 and 0 V, respectively (see Supporting Information Figure S2d).

The total electric displacements derived from one *I*–*V* cycle of both 125 and 500 nm samples are presented in Figure 3c in the form of *D*–*E* curves. The *D*–*E* loop of the 500 nm PLZT film is very similar to the conventional *P*–*E* loop shown in

Figure 2a, with comparable P_r (3.6 $\mu C/cm^2$), E_c (24 kV/cm), and P_{max} (~18 $\mu C/cm^2$). Interestingly, the $D-E$ loop of the 125 nm PLZT film is significantly suppressed, showing smaller values for P_r (0.63 $\mu C/cm^2$), E_c (15 kV/cm), and P_{max} (~6.1 $\mu C/cm^2$). The forward and reverse curves come close to forming a straight line. The small loop is attributed to the small ferroelectric waves and the small leakage current in the $I-V$ curve superimposed on the dominant dielectric box. Clearly, the 125 nm PLZT film behaves closer to a linear dielectric capacitor while the 500 nm PLZT film is dominated by relaxor-ferroelectric properties. The P_r and E_c values at the same E_{max} show approximately a linear relationship with the PLZT film thickness (see Supporting Information Figure S4).

As shown in Figure 4a, the total electric displacement value D per unit of lateral area derived from the $I-V$ measurements

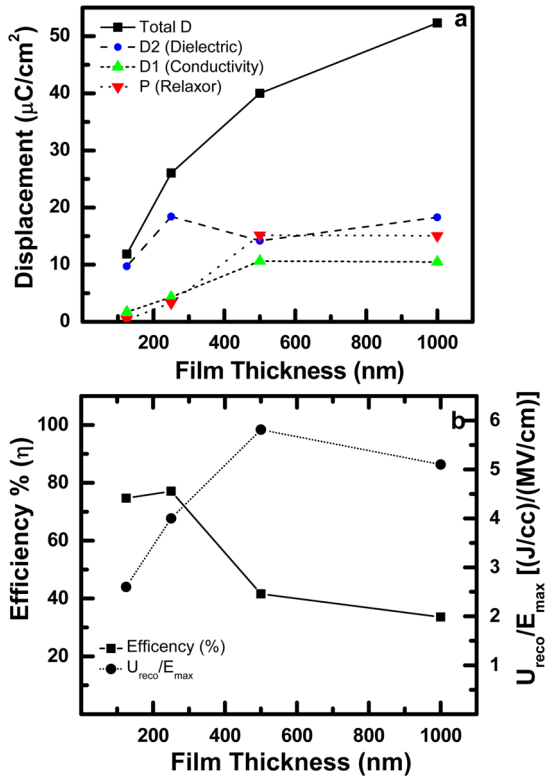

Figure 4. (a) Total electric displacement D and the contributions from electric conductivity $D1$, linear dielectric capacitance $D2$, and relaxor-ferroelectric domain switching polarization P versus the film thickness. (b) The energy storage efficiency and volumetric density (J/cc) normalized with the max electric field strength E_{max} (MV/cm) for different PLZT film thicknesses.

at the E_{max} = 160 kV/cm monotonically increases from ~12 to ~52 $\mu C/cm^2$ as the PLZT film thickness is increased from 125 to 1000 nm. The rate of increase reduces as the thickness becomes larger. Furthermore, the contributions by $D1$, $D2$, and P show very different dependence on the film thickness. In theory, the leakage displacement $D1$ at the same E_{max} (=160 kV/cm) should linearly increase with the film thickness d due to the Ohmic relationship $D1 = (E_{max}^2/\rho v)d$ if the resistivity ρ is a constant for each thickness. The data for the films is consistent with this assumption with the exception of the 1000 nm PLZT film. The dielectric displacement $D2$, on the other hand, is expected to be independent of the film thickness as defined by $D2 = C_0V_{max} = \varepsilon_0\varepsilon_rE_{max}$ if the dielectric permittivity ε_r is a constant over all thicknesses. This assumption appears valid for the observed $D2$ values which randomly vary within ±4 $\mu C/cm^2$ from an average value of ~15 $\mu C/cm^2$. The relaxor-ferroelectric polarization P shows the largest change versus film thickness in concert with the $D1$ value. At 125 nm, there is minimum domain switching and negligible P value. This may be attributed to two factors: (1) suppression of domain wall motion by the mechanical strain/stress from substrate clamping and pinning of grain boundaries, and (2) the effects from an interfacial layer, as reported in a thickness dependence study of $BiFeO_3$ ferroelectric films.[8] The P value jumps to 15.2 $\mu C/cm^2$ for the 500 nm PLZT film and slightly drops to 14.9 $\mu C/cm^2$ for the 1000 nm PLZT film. These values correlate well with the area under the broad $I-V$ wave curves in Figure 3a,b and Supporting Information Figure S2. Overall, the 1000 nm PLZT film shows the highest total displacement D.

For energy storage applications, the high displacement value needs to be supported through high volumetric recoverable density U_{reco} and high energy storage efficiency η, which can be calculated with eqs 1 and 2, respectively. Due to the film thickness, the E_{max} in this study was set at ~160 kV/cm, just below the breakdown field E_b as shown in Supporting Information Figure S3. Since it is known that U_{reco} is linearly proportional to E_{max},[3,12] the normalized value U_{reco}/E_{max} (i.e., the proportional coefficient) is plotted in Figure 4b for ease of comparison with previous studies using much higher E_{max} on thicker films.[3,12] The 500 and 1000 nm PLZT films show much higher U_{reco}/E_{max} values than those at 125 and 250 nm, at 5.8 and 5.1, (J/cc)/(MV/cm), respectively. These values are not far from 11.9 and 13.3 [(J/cc)/(MV/cm)] with sol–gel deposited PLZT films of 3 and 1 μm thickness, respectively.[3,12] On the other hand, the thinner films show much higher energy storage efficiency at 75% (125 nm) and 77% (250 nm) compared to thicker films at 42% (500 nm) and 34% (1000 nm). There is a clear transition in energy storage efficiency from 250 to 500 nm thickness in correspondence with changing from close to linear dielectric properties to nonlinear relaxor-ferroelectrics.

CONCLUSION

It has been shown that the energy storage properties of the thin PLZT films deposited using pulsed laser deposition can be optimized by tuning the film thickness. Cyclic $I-V$ measurements were used to determine the electric displacement and evaluate the contributions from electric conductivity, linear dielectric displacement, and nonlinear relaxor-ferroelectric domain switching. The $D-E$ hysteresis loops constructed by integrating the charge under the $I-V$ curves show consistent features with conventional $P-E$ loops with characteristic coercive field and remnant polarization of relaxor-ferroelectric materials. As the film thickness increases from 125 to 1000 nm, the PLZT film shifts from the behavior close to that of a linear dielectric to relaxor-ferroelectric properties. The thicker PLZT films at 500 and 1000 nm thickness show much higher recoverable energy storage density, but thinner films (at 125 and 250 nm) present higher energy efficiency. There is a trade-off between the linear dielectric properties and nonlinear relaxor-ferroelectric properties for electrical energy storage. Future work on temperature dependence of the PLZT thin films and study of larger film thickness will be used to further optimize this material for solid-state energy storage system.

■ ASSOCIATED CONTENT

Supporting Information

Representative $P-E$ hysteresis loop measured with a conventional Radiant Premier II tester at 100 Hz and the dielectric property as a function of bias electric field for the 500 nm PLZT film. Representative $I-V$ curves measured at a cycling rate of 2000 V/s for all four PLZT film thicknesses, for quick comparison. An $I-V$ curve of the 125 nm PLZT film with a widened electric field E range to demonstrate the dramatic increase in leakage current as E exceeds 160 kV/cm (corresponding to the breakdown field E_b). The characteristic values of remnant polarization P_r and coercive electric field E_c (measured by $I-V$ cycling) versus PLZT film thicknesses, all values normalized to those at a maximum electric field strength of 160 kV/cm. This material is available free of charge via the Internet at http://pubs.acs.org.

■ AUTHOR INFORMATION

Corresponding Authors

*E-mail: jwu@ku.edu.
*E-mail: junli@ksu.edu.

Notes

The authors declare no competing financial interest.

■ ACKNOWLEDGMENTS

This work was supported by NASA Grant NNX13AD42A and NSF EPSCoR Award EPS-0903806 (including the matching support from the State of Kansas through Kansas Technology Enterprise Corporation).

■ REFERENCES

(1) Yao, K.; Chen, S.; Rahimabady, M.; Mirshekarloo, M. S.; Yu, S.; Tay, F. E. H.; Sritharan, T.; Lu, L. Nonlinear Dielectric Thin Films for High-Power Electric Storage with Energy Density Comparable with Electrochemical Capacitors. *IEEE Trans. Ultrason., Ferroelectr., Freq. Control* **2011**, *58*, 1968−1974.

(2) Ogihara, H.; Randall, C. A.; Trolier-McKinstry, S. High-Energy Density Capacitors Utilizing 0.7 $BaTiO_3$-0.3 $BiScO_3$ Ceramics. *J. Am. Ceram. Soc.* **2009**, *92*, 1719−1724.

(3) Tong, S.; Ma, B.; Narayanan, M.; Liu, S.; Koritala, R.; Balachandran, U.; Shi, D. Lead Lanthanum Zirconate Titanate Ceramic Thin Films for Energy Storage. *ACS Appl. Mater. Interfaces* **2013**, *5*, 1474−80.

(4) Dang, Z.-M.; Lin, Y.-H.; Nan, C.-W. Novel Ferroelectric Polymer Composites with High Dielectric Constants. *Adv. Mater.* **2003**, *15*, 1625−1629.5.

(5) Poulsen, M.; Ducharme, S. Why Ferroelectric Polyvinylidene Fluoride is Special. *IEEE Trans. Dielectr. Electr. Insul.* **2010**, *17*, 1028−1035.6.

(6) Zhu, L.; Wang, Q. Novel Ferroelectric Polymers for High Energy Density and Low Loss Dielectrics. *Macromolecules* **2012**, *45*, 2937−2954.

(7) Damjanovic, D. Hysteresis in Piezoelectric and Ferroelectric Materials. In *The Science of Hysteresis*; Bertotti, G., Mayergoyz, I., Eds.; Elsevier: New York, 2005; Chapter 4.

(8) Tang, X.; Dai, J.; Zhu, X.; Lin, J.; Chang, Q.; Wu, D.; Song, W.; Sun, Y.; Tan, X. Thickness-Dependent Dielectric, Ferroelectric, and Magnetodielectric Properties of $BiFeO_3$ Thin Films Derived by Chemical Solution Deposition. *J. Am. Ceram. Soc.* **2012**, *95*, 538−544.

(9) Cross, L. E. Relaxor Ferroelectrics. In *Piezoelectricity*; Springer: Berlin, 2008; pp 131−155.

(10) Ortega, N.; Kumar, A.; Scott, J. F.; Chrisey, D. B.; Tomazawa, M.; Kumari, S.; Diestra, D. G.; Katiyar, R. S. Relaxor-Ferroelectric Superlattices: High Energy Density Capacitors. *J. Phys.: Condens. Matter* **2012**, *24*, 445901.

(11) Hao, X. A Review on the Dielectric Materials for High Energy-Storage Application. *J. Adv. Dielectr.* **2013**, *03*, 1330001.

(12) Hao, X.; Wang, Y.; Yang, J.; An, S.; Xu, J. High Energy-Storage Performance in $Pb_{0.91}La_{0.09}(Ti_{0.65}Zr_{0.35})O_3$ Relaxor Ferroelectric Thin Films. *J. Appl. Phys.* **2012**, *112*, 114111.

(13) Liu, S. Y.; Chua, L.; Tan, K. C.; Valavan, S. E. Novel Ferroelectric Capacitor for Non-Volatile Memory Storage and Biomedical Tactile Sensor Applications. *Thin Solid Films* **2010**, *518*, e152−e155.

(14) Wang, Z. J.; Cao, Z. P.; Otsuka, Y.; Yoshikawa, N.; Kokawa, H.; Taniguchi, S. Low-Temperature Growth of Ferroelectric Lead Zirconate Titanate Thin Films Using the Magnetic Field of Low Power 2.45 GHz Microwave Irradiation. *Appl. Phys. Lett.* **2008**, *92*, 222905.

(15) Shung, K. K.; Cannata, J. M.; Zhou, Q. F. Piezoelectric Materials for High Frequency Medical Imaging Applications: A Review. *J. Electroceram.* **2007**, *19*, 141−147.

(16) Ma, B.; Narayanan, M.; Liu, S.; Chao, S.; U, B. *Ferroelectric PLZT Films Grown on Metal Foils for Power Electronics Applications*. Energy Systems Division, Argonne National Laboratory.: Argonne, IL.

(17) Scarisoreanu, N.; Dinescu, M.; Craciun, F.; Verardi, P.; Moldovan, A.; Purice, A.; Galassi, C. Pulsed Laser Deposition of Perovskite Relaxor Ferroelectric Thin Films. *Appl. Surf. Sci.* **2006**, *252*, 4553−4557.

(18) Tyunina, M.; Levoska, J.; Sternberg, A.; Leppävuori, S. Relaxor Behavior of Pulsed Laser Deposited Ferroelectric $(Pb_{1-x}La_x)$-$(Zr_{0.65}Ti_{0.35})O_3$ Films. *J. Appl. Phys.* **1998**, *84*, 6800.

(19) Ma, C.; Ma, B.; Mi, S.-B.; Lui, M.; Wu, J. Enhanced Dielectric Nonlinearity in Epitaxial $Pb_{0.92}La_{0.08}Zr_{0.52}Ti_{0.48}O_3$ Thin Films. *Appl. Phys. Lett.* **2014**, *104*, 162902−5.

(20) Lee, K.; Rhee, B. R. Leakage Current-Voltage Characteristics of Ferroelectric Thin Film Capacitors. *J. Korean Phys. Soc.* **2001**, *38*, 723−8.

(21) Meyer, R.; Waser, R.; Prume, K.; Schmitz, T.; Tiedke, S. Dynamic Leakage Current Compensation in Ferroelectric Thin-Film Capacitor Structures. *Appl. Phys. Lett.* **2005**, *86*, 142907.

(22) Yan, H.; Inam, F.; Viola, G.; Ning, H.; Zhang, H.; Jiang, Q.; Zeng, T. A. O.; Gao, Z.; Reece, M. J. The Contribution of Electrical Conductivity, Dielectric Permittivity and Domain Switching in Ferroelectric Hysteresis Loops. *J. Adv. Dielectr.* **2011**, *01*, 107−118.

(23) Bobnar, V.; Uršič, H.; Casar, G.; Drnovšek, S. Distinctive Contributions to Dielectric Response of Relaxor Ferroelectric Lead Scandium Niobate Ceramic System. *Phys. Status Solidi B* **2013**, *250*, 2232−2236.

(24) Pike, G. E.; Warren, W. L.; Dimos, D.; Tuttle, B. A.; Ramesh, R.; Lee, J.; Keramidas, V. G.; Evans, J. T. Voltage Offsets in $(Pb,La)(Zr,Ti)O_3$ Thin Films. *Appl. Phys. Lett.* **1995**, *66*, 484.

(25) Zheng, Y.; Wang, B.; Woo, C. H. Effects of Strain Gradient on Charge Offsets and Pyroelectric Properties of Ferroelectric Thin Films. *Appl. Phys. Lett.* **2006**, *89*, 062904.